Design and control of a MAGLEV platform for positioning in arbitrary orientations

Daniel Wertjanz, Ernst Csencsics, Johannes Schlarp and Georg Schitter

***Abstract*— This paper presents the design, control and evaluation of a magnetically levitated six degree of freedom (DoF) positioning platform for robot-based inline measurements of free-form surfaces. The positioning system employs eight voice coil actuators (VCAs) for actuation and is capable of maintaining a constant free-floating position of the mover with respect to its supporting frame in arbitrary orientations of the entire system. Based on a balanced design, low crosstalk between the DoFs is obtained and six decentralized model-based PID controllers are designed and implemented. By using the position signals of six optical proximity sensors with sub-micrometer resolution as feedback, the prototype system achieves a closed-loop control bandwidth higher than 100 Hz for each DoF. The translational and rotational positioning ranges are about $\pm$180 µm and $\pm$2 mrad, respectively. Steady-state rms positioning errors between 142 and 262 nm for the translational DoFs are achieved. Motion experiments show the successful operation of the positioning system in arbitrary orientations, keeping positioning errors below 5 µm/40 µrad.**

I. Introduction

Measurements of surfaces directly in the production line offers the opportunity of a permanent quality assurance of industrial goods. Typical applications can be found in the semiconductor and automotive industry [1], [2]. In surface metrology properties such as flatness, roughness or morphology of a work-piece as well as the deviation from its desired shape are measured [3]. For reasons of efficiency and throughput, measurements for industrial production are required to be fast, precise, robust, and ideally integrated into the production line [4]. Inline measurements is thus a key factor for future industrial production [5]. One major challenge of inline measurements at high resolution in an industrial environment are floor vibrations caused by working machines and other processes. These vibrations can get transmitted to the measuring tool and sample through rigid-body connections, causing motion blur in all degrees of freedom (DOFs) [6] and disturbing measurements at the sub-micrometer scale [7]. Currently, vibration isolation (VI) in industrial nano-metrology is applied by means of passive and active VI strategies [8], and requires an interruption of production to perform quality measurements. Therefore, high precision tools are hardly used within production lines [7].

Recently, a robot-based approach in the field of inline surface inspection has been proposed [9]–[12]. In this concept a measuring device is mounted on a magnetic levitation (MAGLEV) platform which is carried by a robot arm. Instead of isolating both, the measuring tool and the sample, active VI is realized by establishing an artificially stiff link between sample and measurement device by means of feedback control, maintaining a constant distance between the measurement device and the surface to be inspected. However, the operability of the proposed approach is limited to horizontal orientation of the MAGLEV measurement platform, due to the the passive gravity compensation based on a permanent magnet array. To enable surface measurements of free-forms, the MAGLEV measurement platform needs to be actuated and positioned in six DoFs, without a fixed orientation of gravity compensation. A high number of six DoF MAGLEV positioning platform designs has been proposed in the last decades, such as in [13]–[15], but all showing a preferred operation orientation.

The contribution of this paper is the design and control of a MAGLEV positioning platform which is capable of maintaining a desired free-floating position in six DoFs, independent of its orientation.

In Section II the system concept of robot-based high precision measurements of free-forms is presented. The platform design is described in Section III, including the mechanical design, as well as the actuation and sensor system. A mathematical model of the system dynamics, which form the basis for the subsequent control design, are derived in Section IV. Section V discusses the identification of the real system dynamics. Feedback control is designed and implemented in Section VI. Section VII evaluates and demonstrates the system performance, while Section VIII concludes the paper.

II. System concept and requirements

Considering the concept of robot-based free-form surface measurements directly in a production line, a positioning platform is required, which is capable of carrying a measurement tool and align it in arbitrary orientations. To compensate for relative motion between measurement tool and the sample, caused by e.g. floor vibrations, the platform maintains a constant distance and orientation to the sample surface [12].

As a first step towards the introduced concept, this work focuses on the design and control of a MAGLEV positioning platform, which is capable of maintaining a desired free-floating position in six DoFs relative the supporting frame, as shown in Fig. 1. The operability of the platform's internal position control is required to be independent on the orientation and the pose of the robot arm. To enable the prospective compensation for relative motion between the measurement tool and the sample surface, sufficient actuation

The authors are with the Christian Doppler Laboratory for Precision Engineering for Automated In-Line Metrology, Automation and Control Institute (ACIN), Technische Universität Wien, 1040 Vienna. Corresponding author: wertjanz@acin.tuwien.ac.at

Post-print version of the article: D. Wertjanz, E. Csencsics, J. Schlarp, and G. Schitter, "Design and control of a MAGLEV platform for positioning in arbitrary orientations", *2020 IEEE/ASME International Conference on Advanced Intelligent Mechatronics (AIM)*, 2020. DOI: 10.1109/AIM43001.2020.9158898

range in the translational and rotational DoFs is desirable [12]. Therefore, a targeted translational and rotational range of $\pm 100\,\mu\mathrm{m}$ and $\pm 4\,\mathrm{mrad}$, respectively, is set. A control bandwidth of $>100\,\mathrm{Hz}$ [6] is desired for the prospective tracking task of the platform in an industrial environment (see Fig. 1). Moreover, the platform should be capable of carrying a measurement tool of about $0.5\,\mathrm{kg}$, while the total system mass should not exceed the maximum payload of a typical medium-sized industrial robot ($5\,\mathrm{kg}$) [16].

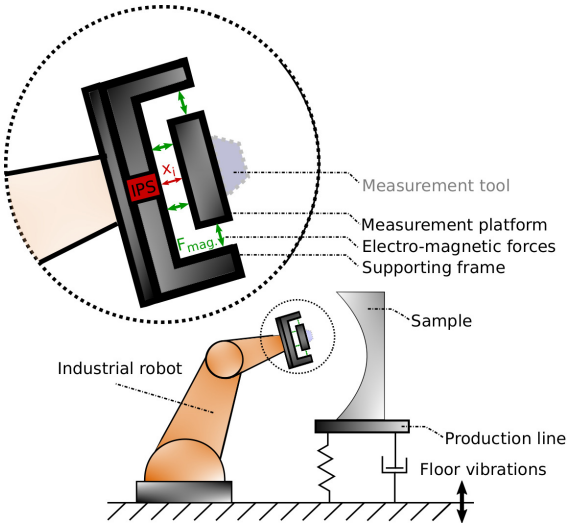

Fig. 1: System concept of robot-based inline measurements of free-form surfaces. A magnetically levitated six DoFs platform enables precise positioning of a measurement tool in arbitrary orientations and poses of the robot arm. An internal position sensor system (IPS) is used to determine the platform position x_i with respect to the supporting frame.

III. Platform Design

To enable mechanical decoupling between the supporting frame and the positioning platform, voice coil actuators (VCAs) are chosen for implementing the (quasi-)zero-stiffness actuation system [17]. Facing the major challenge of the actuators being required to levitate the weight of the entire platform in an arbitrary orientation, a directional gravity compensation based on permanent magnet assemblies [12] is not expedient, which requires a high actuation force of the actuators.

A. Actuation System

Figure 2 presents the design of the MAGLEV positioning platform embedded into a supporting frame. Purely based on Lorentz force, conventional VCAs (VCAR0087-0062-00A, Supt-Motion, Suzhou, China) are utilized for actuation in all DoFs. VCAs provide the major advantage of a linear current to force relation (quasi-zero-stiffness) as well as relatively high peak forces. Hence, bi-directional forces (push and pull) can be applied by using this actuation principle.

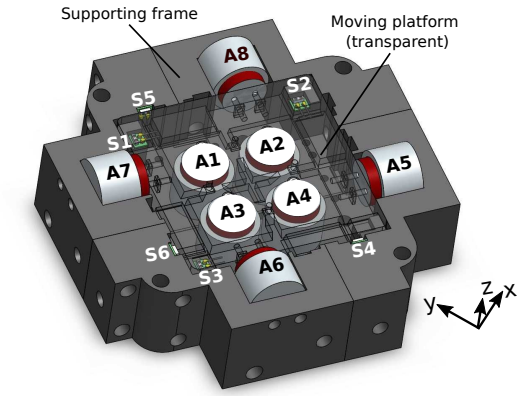

Fig. 2: Six DoF positioning platform with transparent mover. The actuation is done by eight VCAs. Six displacement sensors are used to determine the relative position of the platform to the supporting frame.

The chosen VCA type shows a relatively large air gap of $0.5\,\mathrm{mm}$ between coil and magnet assembly and is capable of applying a continuous force of $20\,\mathrm{N}$. Referring to the actuator placement presented in Fig. 2, achievable positioning ranges for translational and rotational DoFs are $\pm 500\,\mu\mathrm{m}$ and $\pm 4\,\mathrm{mrad}$, respectively, when neglecting mounting tolerances. Good decoupling of the axes is ensured by a symmetric design, avoiding unintended torsional motion through actuation and keeping the subsequent control effort at a low level [18]. Therefore, the eight coils of the identical VCAs are arranged such that the mover's center of mass remains on the z-axis (Fig. 2) and is shifted to the same height as the lateral coils are mounted. The proposed system design is deliberately over-actuated, providing higher peak forces, a symmetric design and the arbitrary operation orientation of the entire system. Being placed beneath the platform the actuators A_1-A_4 are used to apply forces in the out-of-plane directions z, ϕ_x and ϕ_y. The actuators mounted in xy-plane A_5-A_8 enable the positioning of the platform in the in-plane directions x, y and ϕ_z.

To drive the actuators, a custom-made voltage controlled current amplifier is applied. A proportional-integral (PI) controller is implemented as analog circuit by using low noise amplifiers. Based on a high-power operational amplifier (OPA544T, Burr-Brown, Tucson, Arizona, United States), the amplifier is capable of providing $\pm 4\,\mathrm{A}$ continuous current. The PI controller gains are adjusted to the actuator's inductance and series resistance for a current controller bandwidth of $10\,\mathrm{kHz}$ in order to avoid phase lag at the desired position control bandwidth.

B. Internal Sensor System

In order to enable the internal stabilization of the platform with respect to the supporting frame, the platform design includes six displacement sensors to determine the actual

Post-print version of the article: D. Wertjanz, E. Csencsics, J. Schlarp, and G. Schitter, "Design and control of a MAGLEV platform for positioning in arbitrary orientations", *2020 IEEE/ASME International Conference on Advanced Intelligent Mechatronics (AIM)*, 2020. DOI: 10.1109/AIM43001.2020.9158898

position of the platform in all DoFs. Based on optical proximity sensors (HSDL-9100, Avago Technologies, San José, California, United States), a custom-made readout circuit is designed. For the sake of high reflectivity and a higher signal to noise ratio, highly reflective tape is attached on the target points. Each sensor channel is calibrated by an external interferometric sensor system (IDS3010, attocube - Wittenstein Group, Germany). The sensor characteristics are fitted by a fifth order polynomial between distances of 1 and 2.8 mm, achieving a resolution of about 200 nm (rms positioning noise). To attenuate noise occurring at higher frequencies, a low-pass filter at the sensor output is set to a cut-off frequency of 10 kHz. In Figure 2 the proposed sensor placement is shown, which ensures observability of all DoFs. A set of three sensors S_1, S_2 and S_3, placed on three edges beneath the platform, is used to determine the position in directions of z, ϕ_x and ϕ_y. The second set of sensors S_4, S_5 and S_6 are utilized to measure displacements in x, y and ϕ_z.

C. Mechanical Structure

The mechanical design of the quadratic mover is shown in Fig. 3a. It is modelled with a length of 150 mm and a maximum height of 16 mm. A cross strut is included fulfilling two major tasks. Firstly, higher stiffness of the overall mover is achieved, such that structural modes are shifted to higher frequencies. Secondly, the additional mass of the cross strut chosen such that the center of mass is in-plane with the actuators mounted in the xy-plane, which allows to avoid unintended torsional motion. Regarding the mounting distance of the VCAs relative to the center of the frame, a trade-off between maximum range and maximum torque of the rotational DoFs has to be made. Placing the actuators closer to the edges of the mover would increase the achievable torque but decrease the maximum actuation range. For the sake of rapid prototyping and lightweight mover design, the mechanical components, i.e. the supporting frame and the moving platform, are 3D printed. The utilized filament is polyethylene terephthalate glycol-modified (PET-G), showing a density and Young's modulus of 1.27 g cm^{-3} and 2.2 GPa, respectively. The mass of one coil assembly is 46 g, resulting in a total moving mass of 692 g. Using geometry and the material properties, structural modes of the designed platform are calculated by utilizing ANSYS Mechanical (ANSYS, Canonsburg, Pennsylvania, United States).
Figure 3b shows the FEM simulation results. The first structural mode is expected at 322 Hz which is about 200 Hz higher than the desired closed-loop control bandwidth. This mode shape is indicated by a bending of the edges on which the coils are mounted. If this structural mode is excited by actuation, a band-stop filter may be applicable to ensure its attenuation. The real system dynamics are analyzed and discussed later in Section V.

D. Experimental Setup Overview

The supporting frame and positioning platform, presented in Section III-C, are manufactured by 3D printing for reasons

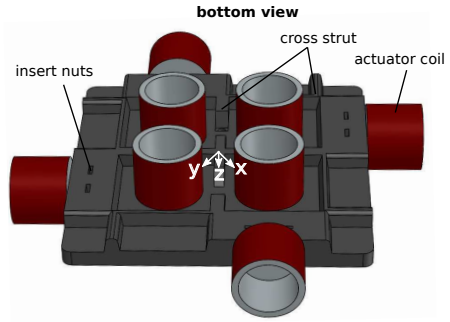

(a)

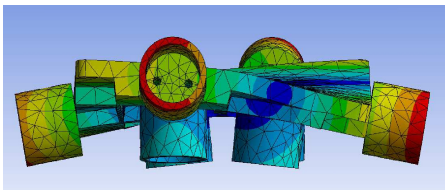

(b)

Fig. 3: Levitated mover design. (a) The coils of the eight VCAs are mounted beneath and around the mover. A cross strut ensures higher stiffness. (b) First structural mode shape of the moving platform at 322 Hz resulting from an FEM modal analysis.

of a lightweight mover design and high design flexibility. PET-G is used as filament, yielding a total moving mass of 692 g. The supporting frame consists of four identical parts, each including five insert nuts enabling an assembly by screw connection. In addition, the assembled frame provides four sensor places beneath and eight around the platform. At its widest point the supporting frame is 264 mm with a height of 64 mm. The mass of the total system is about 4.3 kg.

The experimental setup is shown in Fig. 4, including the manufactured and assembled prototype, the custom-made actuation and sensor system as well as the hardware interface of the rapid prototyping system. In order to stabilize and position the platform, a cascaded control strategy is implemented. The outer position controller is implemented on development tools of Beckhoff Automation GmbH & Co. KG, which allow rapid prototyping and automated measurements. A bus cycle time of 50 µs is set, which is equivalent to a sampling frequency of 20 kHz. The inner analog current control loop (10 kHz) applies the desired current to the VCAs.

IV. System Modelling

The actuation in the out-of-plane DoF is a superposition of the forces generated by the four VCAs A_1-A_4 (see Fig. 2). In contrast, A_5-A_8 enable the actuation of the platform in-plane. The gravitational force is needed to be compensated in arbitrary orientations of the platform, which requires an orientation-dependent offset current for each VCA. Dynamics related to position changes of the entire systems

Post-print version of the article: D. Wertjanz, E. Csencsics, J. Schlarp, and G. Schitter, "Design and control of a MAGLEV platform for positioning in arbitrary orientations", *2020 IEEE/ASME International Conference on Advanced Intelligent Mechatronics (AIM)*, 2020. DOI: 10.1109/AIM43001.2020.9158898

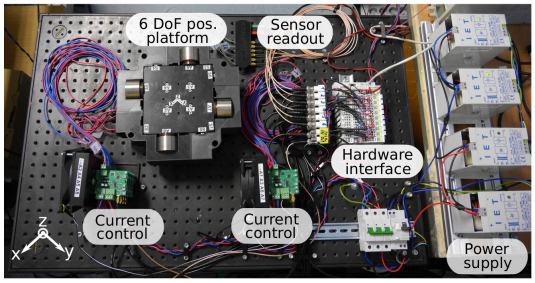

Fig. 4: Experimental setup overview.

are neglected, assuming sufficiently low accelerations when moving the entire system. Due to (quasi)-zero-stiffness actuation, the state-space representation of the dynamic system can be written as floating mass model

$$\ddot{\zeta} = \begin{bmatrix} \ddot{x} \\ \ddot{y} \\ \ddot{z} \\ \ddot{\phi}_x \\ \ddot{\phi}_y \\ \ddot{\phi}_z \end{bmatrix} = \mathbf{A}\mathbf{i} = \mathbf{A} \begin{bmatrix} i_x \\ i_y \\ i_z \\ i_{\phi_x} \\ i_{\phi_y} \\ i_{\phi_z} \end{bmatrix}, \tag{1}$$

with the actual acceleration of the platform $\ddot{\zeta}$, the dynamic matrix $\mathbf{A}$ and the actual current values represented by the current vector $\mathbf{i}$. Assuming the DoFs being decoupled by design, crosstalk is initially neglected and identified in Section V. Thus, the dynamic matrix

$$\mathbf{A} = \begin{bmatrix} \frac{4k_m}{\sqrt{2}m} & 0 & 0 & 0 & 0 & 0 \\ 0 & \frac{4k_m}{\sqrt{2}m} & 0 & 0 & 0 & 0 \\ 0 & 0 & \frac{4k_m}{m} & 0 & 0 & 0 \\ 0 & 0 & 0 & \frac{2k_m l_x}{I_x} & 0 & 0 \\ 0 & 0 & 0 & 0 & \frac{2k_m l_y}{I_y} & 0 \\ 0 & 0 & 0 & 0 & 0 & \frac{4k_m l_z}{I_z} \end{bmatrix} \tag{2}$$

has only entries in the main diagonal, with m representing the total mover mass, k_m the motor constant of the VCAs, l_x, l_y and l_z the lever arms of torque and I_x, I_y and I_z the moments of inertia in the rotational directions. In Tab. I these parameters are summarized.

TABLE I: Parameters of system dynamics.

Parameter	Value	Description
m	0.7 kg	Total moving mass
k_m	12.7 N A^{-1}	Motor constant of VCA
l_x	$\sqrt{2}$ 25 mm	Lever of torque in direction ϕ_x
l_y	$\sqrt{2}$ 25 mm	Lever of torque in direction ϕ_y
l_z	25 mm	Lever of torque in direction ϕ_z
I_x	1.3 m kg	Moment of inertia in direction ϕ_x
I_y	1.3 m kg	Moment of inertia in direction ϕ_y
I_z	2.5 m kg	Moment of inertia in direction ϕ_z
τ_d	138 µs	Time delay of rapid prototyping system

Currents required to apply translational forces, resulting in accelerations in x-, y- and z-direction, are determined by the mover mass and the motor constant of the actuators. In contrast, angular accelerations depend on the moments of inertia about the axes, as well as the levers of torque and the forces generated for given currents. The current in the eight actuator coils $\mathbf{i_a} = \begin{bmatrix} i_1 & i_2 & i_3 & i_4 & i_5 & i_6 & i_7 & i_8 \end{bmatrix}^T$ is a superposition according to $\mathbf{i_a} = \mathbf{T}\mathbf{i}$, with

$$\mathbf{T} = \frac{1}{4} \begin{bmatrix} 1 & 2 & 0 & 0 & 0 & 0 \\ 1 & 0 & -2 & 0 & 0 & 0 \\ 1 & 0 & 2 & 0 & 0 & 0 \\ 1 & -2 & 0 & 0 & 0 & 0 \\ 0 & 0 & 0 & -1 & 1 & -1 \\ 0 & 0 & 0 & 1 & 1 & -1 \\ 0 & 0 & 0 & 1 & -1 & -1 \\ 0 & 0 & 0 & -1 & -1 & -1 \end{bmatrix} \tag{3}$$

being a linear transformation matrix. The actual position ζ of the moving platform is a non-linear function of the measured sensor signals $\zeta = \mathbf{h}(\mathbf{d})$, with $\mathbf{h}(\mathbf{d})$ being a set of trigonometric functions obtained from the system geometry and depending on the displacements $\mathbf{d} = [d_1, d_2, d_3, d_4, d_5, d_6]$ measured by the optical proximity sensors. The system equations in state-space representation and the output equation are given as

$$\ddot{\zeta} = \mathbf{A}\mathbf{i} \tag{4a}$$
$$\zeta = \mathbf{h}(\mathbf{d}) \tag{4b}$$

V. System Identification

Due to the magnetic levitation based actuation, the dynamic system behaviour can not simply be measured in an open-loop manner. To identify the exact system dynamics, the whole system first needs to be stabilized in a defined operating point. Therefore, controllers for closed-loop identification of all DoFs are required. Based on the mathematical model of the system, one low-bandwidth (50 Hz) single-input single-output (SISO) proportional-integral-derivative (PID) controller for the identification of each DoF is designed and implemented in a first step [17]. After identifying the actual system dynamics, the controllers are adapted and optimized in a second step (Section VI), in order to achieve a high bandwidth. The implementation of this SISO approach is only justified if the crosstalk between axes is sufficiently low. The dynamic behaviour of the existing crosstalk between all DoFs is investigated later in this section. Figure 5 exemplifies the identification of the dynamic system behaviour. Assuming decoupled axes ($G_{yx} = 0$) and feedback control for each DoF, the input sensitivity and complementary sensitivity are given by $U_x = \frac{u_x}{x_r} = \frac{C_x}{1+C_xG_x}$ and $T_x = \frac{x}{x_r} = \frac{C_xG_x}{1+C_xG_x}$, respectively. The plant to be identified G_x is obtained by dividing T_x by U_x.

A system analyzer (3562A, Hewlett-Packard, Palo Alto, CA, USA) is used to measure the complementary and input sensitivity transfer functions. With the purpose of identifying

Post-print version of the article: D. Wertjanz, E. Csencsics, J. Schlarp, and G. Schitter, "Design and control of a MAGLEV platform for positioning in arbitrary orientations", *2020 IEEE/ASME International Conference on Advanced Intelligent Mechatronics (AIM)*, 2020. DOI: 10.1109/AIM43001.2020.9158898

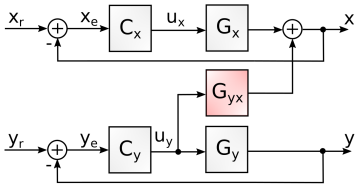

Fig. 5: Simplified block diagram used for the system dynamics in closed-loop position control, schematically shown for DoF x and y.

system dynamics around mid-position of the moving platform, small-signal amplitudes (10 µm and 100 µrad, respectively), are applied.

In order to prove that the SISO PID position control approach is justified, the level of crosstalk between the DoFs is determined. The crosstalk dynamics can again not be measured in open-loop, but only in the feedback-controlled system. Defining crosstalk dynamics exemplarily as the transfer function G_{yx} of one controller output u_y to the position of another DoF x, illustrated in Fig. 5, G_{yx} can be calculated by knowledge of the sensitivity function $S_x = \frac{x}{u_x G_{yx}}$ of the fully controlled system as given by

$$\frac{x}{u_y} = G_{yx}\frac{1}{1+C_xG_x} = G_{yx}S_x \tag{5}$$

$$\rightarrow G_{yx} = \frac{x}{u_y}\frac{1}{S_x}. \tag{6}$$

The overall results of the dynamics identification task, which comprise the six dynamics of each DoF and 30 crosstalk dynamics, would go beyond the scope of this work. However, the crosstalk occurring at low frequencies is 15 to 30 dB lower than the related system dynamics (data not shown) and validates the chosen approach of six SISO PID position controllers.

VI. Control Design and Implementation

Figure 6 exemplary shows the identified dynamics of DoF z (dotted). Aiming to meet the system performance goals and to maximize the positioning control bandwidth, the SISO PID controllers used for the system identification in Section V are re-designed and adapted to the actual dynamics obtained by the system identification. The identified frequency responses of each DoF show first structural modes around 200 Hz, which represent a potential limitation for the achievable control bandwidth. The SISO PID controllers

$$C_{pid} = \frac{k_p}{1+\frac{s}{\omega_t}} + \frac{k_i}{s} + \frac{k_d s}{1+\frac{s}{\omega_t}} \tag{7}$$

are designed in accordance with the design guidelines for low-stiffness systems in [17]. While using the P-gain to shift the loop gain to the desired crossover frequency, the D-gain ensures sufficient phase-lead in this frequency range. In order to ensure stability, a trade-off between control

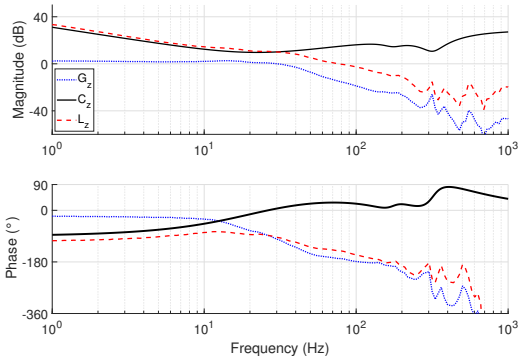

Fig. 6: Control design DoF z. The controller C_z is designed and optimized with respect to the measured system dynamics G_z. The cross-over frequency of 90 Hz, together with the two notch filters at 190 Hz and 310 Hz, result in a robust loop gain L_z (gain margin 7 dB, phase margin 47°).

bandwidth (min. 100 Hz) and preserving a sufficient phase margin of at least 35° is made. A realization term is used to stop the differential action and limit the control effort at higher frequencies. The I-gain increases the loop gain at low frequencies and reduces the steady-state positioning error. To attenuate the resonance peaks of the structural modes at around 250 Hz, two notch filters are used. The transfer function of these filters are given by

$$H_N = \frac{s^2 + \delta 2\pi\nu s + 4\pi^2\nu^2}{s^2 + 2\delta\rho 2\pi\nu s + 4\pi^2\nu^2}, \tag{8}$$

with δ determining the width and ρ the depth of the notch filter at a desired frequency ν. The extended position controller design results to

$$C = C_{pid}H_{N,1}H_{N,2}. \tag{9}$$

As an example, the designed controller for DoF z, together with its system dynamics and the loop gain, is shown in Fig. 6. An open-loop cross-over frequency of 90 Hz is obtained for this DoF. The two notch filters can be seen at 190 Hz and 310 Hz. A gain and phase margin of 7 dB and 47° are achieved, respectively. For the controller implementation on the processor of the rapid prototyping system, the controllers are discretized for a sampling frequency of $f_s = 20$ kHz using pole-zero-matching [19].

VII. Evaluation of System Performance

A. Frequency Responses of Closed-Loop Controlled System

In order to determine the system's frequency response in feedback operation, complementary sensitivity functions of the closed-loop controlled system are determined. While stabilizing the platform in all DoFs, a Bode plot of each axis is measured separately using a system analyzer. For this purpose, small-signal amplitudes of 10 µm and 100 µrad are applied. Nominal operation point is the center-position of

Post-print version of the article: D. Wertjanz, E. Csencsics, J. Schlarp, and G. Schitter, "Design and control of a MAGLEV platform for positioning in arbitrary orientations", *2020 IEEE/ASME International Conference on Advanced Intelligent Mechatronics (AIM)*, 2020. DOI: 10.1109/AIM43001.2020.9158898

the moving platform with respect to the supporting frame. Figure 7 summarizes the results for translational and rotational DoFs. Closed-loop control bandwidths between 100 and 138 Hz are achieved. The implemented control designs including the placement of notch filters between 175 and 500 Hz yield good attenuation of the structural resonance peaks in this frequency range.

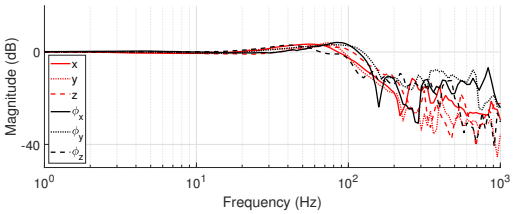

Fig. 7: Complementary sensitivity functions of translational and rotational DoFs. Closed-loop positioning control bandwidths between 100 and 138 Hz can be observed. At higher frequencies good attenuation of the structural resonance peaks is achieved.

B. Positioning Range and Noise

As discussed in Section III-C, the actuation range of the platform is determined by the actuator placement together with manufacturing tolerances. The achieved translational and rotational ranges is around $\pm 180\,\mu\text{m}$ and $\pm 2\,\text{mrad}$, respectively, and summarized in Tab. II. Figure 8 exemplary shows a repositioning in DoFs z and ϕ_x over a range of $360\,\mu\text{m}$ and $4\,\text{mrad}$. Throughout the performed full-range motions the positioning errors tare kept at a low level. By analyzing the steady-state positioning errors, the translational DoFs show an rms positioning noise between $142\,\text{nm}$ and $262\,\text{nm}$, which is about the noise level of the developed optical proximity sensor system (see Section III-B). A summary of the measured rms positioning noise is listed in Tab. II. The out-of-plane DoFs show a lower positioning noise due to the fact, that these sensors are placed beneath the platform yielding a better shielding against background light and, therefore, a higher signal to noise ratio (SNR).

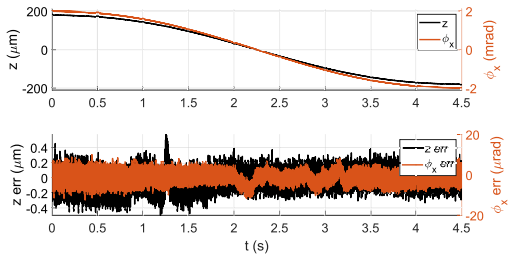

Fig. 8: Full range trajectory of $360\,\mu\text{m}$ and $4\,\text{mrad}$ in DoFs z and ϕ_x, respectively. The positioning error throughout the performed motion is kept below $500\,\text{nm}$ and $10\,\mu\text{rad}$.

TABLE II: Positioning noise of levitated platform.

DoF	Pos. noise (rms)	Pos. range
$x/y/z$	$205/262/142\,\text{nm}$	$\pm 160/\pm 150/\pm 180\,\mu\text{m}$
$\phi_x/\phi_y/\phi_z$	$85.9/73.9/191.6\,\mu\text{deg}$	$\pm 2/\pm 2.09/\pm 1.75\,\text{mrad}$

C. System Performance in Arbitrary Orientations

To demonstrate that the positioning system operates in arbitrary orientation of the supporting frame, the entire prototype is moved between several orientations. The positioning error in steady state and different orientations, with the system mounted on a lab table, is evaluated. As expected, the positioning noise remains constant in all orientations due to the linear actuation principle (values shown in Tab. II).

Finally, the following experiment simulates motions of a robot-based inspection system measuring a free-form surface in order to determine the dynamic positioning error. The series of movements, in which the platform is facing the *wall (1) - floor (2) - ceiling (3) - wall (4)* followed by a *rotation around the z-axis (5)*, is performed in a time span of $13.6\,\text{s}$ and visualized in Fig. 9a. In the starting position with the platform facing the wall, the current to compensate for gravity is spread over the four in-plane actuators (pushing: A_5, A_7; pulling: A_6, A_8), as it can be seen in Fig. 9d. An absolute force in direction of $-x$ according to

$$F_{-x}(t)_{|t=0\,\text{s}} = \frac{k_m}{\sqrt{2}} \sum_{j=5}^{j=8} |i_j| \approx 4 \cdot 12.7\,\text{N}\,\text{A}^{-1} 0.18\,\text{A} = 6.47\,\text{N} \tag{10}$$

is generated. The value of $6.47\,\text{N}$ is expected to compensate gravitational forces on the mover of about $0.7\,\text{kg}$. The out-of-plane actuators require only low current values to stabilize the platform in this position. Transferring the system to orientation 2 with the platform facing the floor, the out-of-plane actuators $A_1 - A_4$ start to pull until the current in the in-plane actuators is close to zero (Fig. 9b). Meanwhile, the positioning errors of DoFs x (Fig. 9e) and z(Fig. 9c) reach a maximum of $4\,\mu\text{m}$ and $5\,\mu\text{m}$, respectively, caused by accelerations occurring in these directions. Comparing the current values in Fig. 9b and Fig. 9d), it can be clearly seen that the energy consumption in orientation 2 is lower by a factor of $\frac{1}{\sqrt{2}}$ than it has been in orientation 1, due to the actuator arrangement. The relation between the resulting motor constants in z- and x-direction and thus the force generated for a given current, as indicated in Eq. 2, is $\frac{k_z}{k_x} = \frac{4k_m}{\frac{4k_m}{\sqrt{2}}} = \sqrt{2}$. Next, the supporting frame is rotated by $-180°$ in ϕ_y in the time interval of $t = [4.5\,\text{s}, 9.5\,\text{s}]$ to orientation 3 (platform facing ceiling). Again, positioning errors of DoFs x and z reach a maximum during this movement due to accelerations in these directions. The following orientation 4 (platform facing the wall) is indicated by nearly zero current for generating force in z direction (out-of-plane actuators), while currents of the lateral actuators reach a distribution equal to the starting orientation ($t = 12.4\,\text{s}$). The last movement is a rotation of $-45°$ around the z-axis. Throughout this motion, the positioning errors of the

Post-print version of the article: D. Wertjanz, E. Csencsics, J. Schlarp, and G. Schitter, "Design and control of a MAGLEV platform for positioning in arbitrary orientations", *2020 IEEE/ASME International Conference on Advanced Intelligent Mechatronics (AIM)*, 2020. DOI: 10.1109/AIM43001.2020.9158898

rotational DoFs are lower than $40\,\mu\text{rad}$ (ϕ_x and ϕ_y) and $50\,\mu\text{rad}$ (ϕ_z). A total current/power of $0.72\,\text{A}/17.3\,\text{W}$ is needed to hover the platform if the gravitation force vector points in DoFs $\pm x$- or $\pm y$-direction. In case of $\pm z$, these values are reduced by a factor of $\frac{1}{\sqrt{2}}$ to $0.51\,\text{A}/12.2\,\text{W}$ due to the actuator placement and chosen coordinate system.

In summary it is shown that the magnetically levitated positioning system operates in arbitrary orientations and keeps the dynamic positioning error lower than $5\,\mu\text{m}/40\,\mu\text{rad}$ during the performed motion experiment. In steady-state an orientation-independent positioning error of about $200\,\text{nm}$ and $1.7\,\mu\text{rad}$ is achieved, with the sensor noise (see Sec. III-B) being the limiting factor.

VIII. Conclusion

In this paper, a magnetically levitated six DoF positioning platform with arbitrary operation orientation is presented. By using eight identical VCAs for the actuation and the position signals of six displacement sensors as feedback, the platform is capable of maintaining a constant free-floating position in six DoFs with respect to the supporting frame. To manufacture the mechanical parts of the system, 3D printing is used, resulting in a low moving mass of the platform of $692\,\text{g}$. The mass of the entire system is about $4.3\,\text{kg}$, which is well within the prototype performance goals for robot-based operation. Over-actuation is deliberately chosen for the sake of a balanced design, with the VCAs arranged to minimize torque and crosstalk between the DoFs, resulting in good decoupling of the axes, enabling a SISO control approach for each DoF. Utilization of six SISO PID controllers and well placed notch filters enables to achieve the targeted control bandwidth of more than $100\,\text{Hz}$. A range of about $\pm 180\,\mu\text{m}$ and $\pm 2\,\text{mrad}$ in translational and rotational directions, respectively, is achieved. Steady-state rms positioning errors between 142 and $262\,\text{nm}$ of the translational DoFs are obtained, which corresponds to the noise of the sensor system. The desired orientation-independent operation of the positioning system is successfully demonstrated by motion experiments during which the dynamic positioning errors remain below $5\,\mu\text{m}/40\,\mu\text{rad}$.

Future work include the integration of external tracking sensors, which measure the distance and orientation between the platform and a sample surface. By maintaining the platform at a constant distance and orientation with respect to the sample surface, relative motion between the tool and the platform can be actively compensated.

ACKNOWLEDGMENT

The financial support by the Christian Doppler Research Association, the Austrian Federal Ministry for Digital and Economic Affairs, and the National Foundation for Research, Technology and Development, as well as MICRO-EPSILON MESSTECHNIK GmbH & Co. KG and ATENSOR Engineering and Technology Systems GmbH is gratefully acknowledged.

References

[1] Arjun Yogeswaran and Pierre Payeur. 3d surface analysis for automated detection of deformations on automotive body panels. In *New Advances in Vehicular Technology and Automotive Engineering*. IntechOpen, 2012.

[2] T.-F. Yao, A. Duenner, and M. Cullinan. In-line dimensional metrology in nanomanufacturing systems enabled by a passive semiconductor wafer alignment mechanism. *Journal of Micro- and Nano-Manufacturing*, 5(1), 2016.

[3] D. J. Whitehouse. *The Handbook of Surface and Nanometrology*. Taylor and Francis, 1 edition, 2002.

[4] Heinrich Schwenke, Ulrich Neuschaefer-Rube, Tilo Pfeifer, and Horst Kunzmann. Optical methods for dimensional metrology in production engineering. *CIRP Annals*, 51(2):685 – 699, 2002.

[5] T. Uhrmann, T. Matthias, M. Wimplinger, J. Burggraf, D. Burgstaller, H. Wiesbauer, and P. Lindner. Recent progress in thin wafer processing. In *2013 IEEE International 3D Systems Integration Conference (3DIC)*, pages 1–8, 2013.

[6] Colin G. Gordon. *Generic Vibration Criteria for Vibration-Sensitive Equipment*. Colin Gordon & Associates, 1999.

[7] M. Thier, R. Saathof, A. Sinn, R. Hainisch, and G. Schitter. Six degree of freedom vibration isolation platform for in-line nano-metrology. *IFAC-PapersOnLine*, 49-21:149–156, 2016.

[8] J. van Eijk, D. Laro, J. Eisinger, W. Aarden, T. Michielsen, and S. van den Berg. The "ultimate performance" in floor vibration isolation. *Mikroniek. Professional Journal on Precision Engineering*, 51:13–19, 2011.

[9] M. Thier, R Saathof, R Hainisch, and G. Schitter. Vibration compensation platform for robot-based nanoscale measurements. *15th International Conference of the EUSPE*, pages 59–71, 2015.

[10] M. Thier, R Saathof, E. Csencsics, R Hainisch, A. Sinn, and G. Schitter. Design and control of a positioning system for robot-based nanometrology. *at- Automatisierungstechnik*, 63:727 – 738, 2015.

[11] Ruijun Deng, Rudolf Saathof, J.W. Spronck, S.A.J. Hol, and Robert H. Munnig Schmidt. Integrated 6-dof lorentz actuator with gravity compensator for precision positioning. *22nd International Conference on Magnetically Levitated Systems and Linear Drives (MAGLEV)*, 2014.

[12] M. Thier, R. Hainisch, G. Schitter, and R. Saathof. Metrology platform to enable in-line nanometrology. *Industrial Technologies, Amsterdam, The Netherlands*, 2016.

[13] Shobhit Verma, Won-jong Kim, and Jie Gu. Six-axis nanopositioning device with precision magnetic levitation technology. *IEEE/ASME Transactions on Mechatronics*, 9:384 – 391, 2004.

[14] H. Zhu, T. J. Teo, and C. K. Pang. Design and modeling of a six-degree-of-freedom magnetically levitated positioner using square coils and 1-d halbach arrays. *IEEE Transactions on Industrial Electronics*, 64(1):440–450, Jan 2017.

[15] V. H. Nguyen and W. Kim. Two-phase lorentz coils and linear halbach array for multiaxis precision-positioning stages with magnetic levitation. *IEEE/ASME Transactions on Mechatronics*, 22(6):2662–2672, Dec 2017.

[16] Bruno Siciliano and Oussama Khatibd. *Springer handbook of robotics*. Springer, 2 edition, 2016.

[17] R Munnig Schmidt, G Schitter, A Rankers, and J van Eijk. *The Design of High Performance Mechatronics*. IOS Press, Amsterdam, 2 edition, 2014.

[18] E. Csencsics, J. Schlarp, and G. Schitter. High-performance hybrid-reluctance-force-based tip/tilt system: Design, control, and evaluation. *IEEE/ASME Transactions on Mechatronics*, 23(5):2494–2502, Oct 2018.

[19] Karl Johan Åström and Björn Wittenmark. *Computer-controlled systems : theory and design (3 ed.)*. Prentice-Hall, 1997.

Post-print version of the article: D. Wertjanz, E. Csencsics, J. Schlarp, and G. Schitter, "Design and control of a MAGLEV platform for positioning in arbitrary orientations", *2020 IEEE/ASME International Conference on Advanced Intelligent Mechatronics (AIM)*, 2020. DOI: 10.1109/AIM43001.2020.9158898

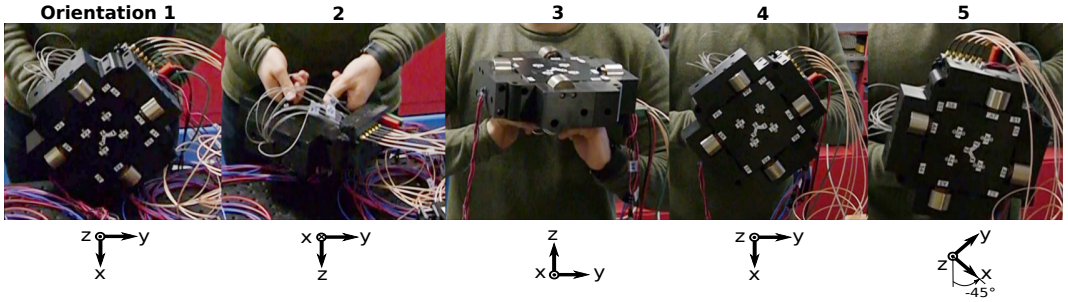

(a) Series of movements over time.

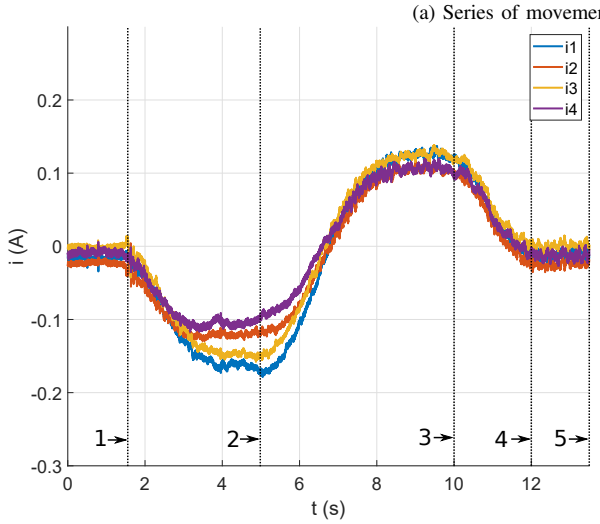

(b) Current distribution over out-of-plane actuators $A1 - A4$.

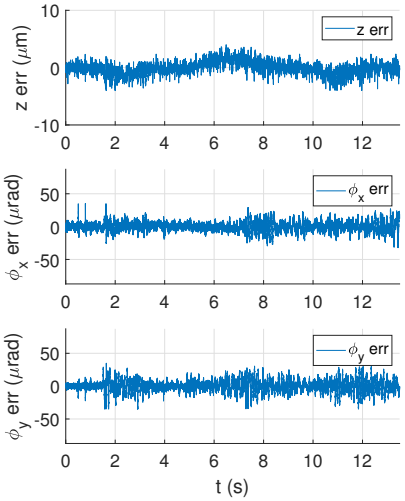

(c) Positioning error of out-of-plane DoFs.

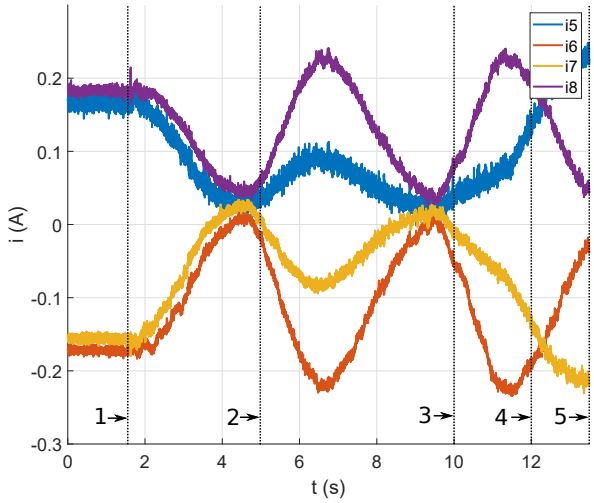

(d) Current distribution over in-plane actuators $A5 - A8$.

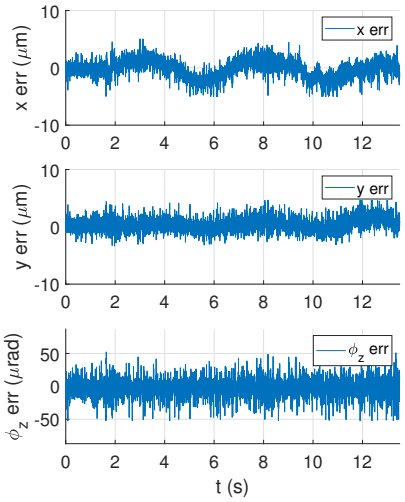

(e) Positioning error of in-plane DoFs.

Fig. 9: Positioning error and current distribution during movements of the entire system to different orientations. (a) illustrates the series of movements over timer. In (b) and (d) the corresponding current distribution (5-point moving average applied) over the out-of-plane and in-plane actuators, respectively, can be seen. (c) and (e) show the positioning errors for all DoF.

Post-print version of the article: D. Wertjanz, E. Csencsics, J. Schlarp, and G. Schitter, "Design and control of a MAGLEV platform for positioning in arbitrary orientations", *2020 IEEE/ASME International Conference on Advanced Intelligent Mechatronics (AIM)*, 2020. DOI: 10.1109/AIM43001.2020.9158898